Flow boiling heat transfer and pressure drop characteristics of R134a, R1234yf and R1234ze in a plate heat exchanger for organic Rankine cycle units

Zhang, Ji; Desideri, Adriano; Kærn, Martin Ryhl; Ommen, Torben Schmidt; Wronski, Jorrit; Haglind, Fredrik

Published in:
International Journal of Heat and Mass Transfer

Link to article, DOI:
10.1016/j.ijheatmasstransfer.2017.01.026

Publication date:
2017

Document Version
Peer reviewed version

Flow boiling heat transfer and pressure drop characteristics of R134a, R1234yf and R1234ze in a plate heat exchanger for organic Rankine cycle units

Ji Zhang[a,*], Adriano Desideri[b], Martin Ryhl Kærn[a], Torben Schmidt Ommen[a], Jorrit Wronski[c], Fredrik Haglind[a]

[a]Department of Mechanical Engineering, Technical University of Denmark, Nils Koppels Allé, Building 403, 2800 Kongens Lyngby, Denmark
[b]Thermodynamics laboratory, University of Liège, Sart-Tilman Campus B49-P33, 4000 Liège, Belgium
[c]IPU, Kongens Lyngby, Denmark

Abstract

The optimal design of the evaporator is one of the key issues to improve the efficiency and economics of organic Rankine cycle units. The first step in studying the evaporator design is to understand the thermal-hydraulic performance of the working fluid in the evaporator of organic Rankine cycles. This paper is aimed at obtaining flow boiling heat transfer and pressure drop characteristics in a plate heat exchanger under the working conditions prevailing in the evaporator of organic Rankine cycle units. Two hydrofluoroolefins R1234yf and R1234ze, and one hydrofluorocarbon R134a, were selected as the working fluids. The heat transfer coefficients and pressure drops of the three working fluids were measured with varying saturation temperatures, mass fluxes, heat fluxes and outlet vapour qualities, which range from 60 °C to 80°C, 86 kg/m^{2}s to 137 kg/m^{2}s, 9.8 kW/m^2 to 36.8 kW/m^2 and 0.5 to 1, respectively. The working conditions covered relatively high saturation temperatures (corresponding reduced pressures of 0.35–0.74), which are prevailing in organic

* Corresponding author. Tel.: +45 45 25 13 87; fax: +45 45 25 19 61
E-mail address: jizhang@mek.dtu.dk (Ji Zhang)

Rankine cycles yet absent in the open literature. The experimental data were compared with existing correlations, and new correlations were developed that are more suitable for evaporation in organic Rankine cycles. The experimental results indicate that heat transfer coefficients are strongly dependent upon the heat flux and saturation temperature. Moreover, the results suggest better thermal-hydraulic performance for R1234yf than the other two working fluids at the same saturation temperatures. With the new heat transfer and pressure drop correlations, agreements within ± 25 % were obtained for experimental data in similar experiments with high saturation temperatures.

Keywords: flow boiling, plate heat exchanger, high saturation temperature, HFO, pressure drop

Nomenclature

Symbols

A	heat transfer area, m^2
b	amplitude of corrugation, m
Bd	Bond number
Bo	Boiling number
c_p	specific heat capacity, J/kg K
D	diameter, m
f	friction factor
G	mass flux, kg/m^2s
h	heat transfer coefficient, W/m^2 K
h_{fg}	enthalpy of evaporation, J/kg
k	thermal conductivity, W/m K
L	length, m
LMTD	log mean temperature difference, °C
M	molecular weight
$\dot{m}$	mass flow rate, kg/s
Nu	Nusselt number
P	pressure, Pa
Pr	Prandtl number
Q	heat transfer rate, W
q	heat flux, W/m^2
Re	Reynolds number
T	temperature, °C
U	overall heat transfer coefficient, W/m^2 K
W	width, m
We	Weber number
x	vapour quality

Subscripts

acc	acceleration
cri	critical
eq	equivalent
eva	evaporator
exp	experimental
fri	frictional
g	gravitational
gra	gradient
h	hydraulic
in	inlet
l	liquid
lo	liquid only
m	mean
oil	oil
out	outlet
p	port
pre	pre-heater
pred	predicted
r	reduced
sat	saturation
tf	two-phase
v	vapour
vo	vapour only
w	water
wall	wall
wf	working fluid

Greek Symbols

γ	dimensionless corrugation parameter
β	chevron angle, °
φ	enlargement factor of corrugation surface
μ	dynamic viscosity, Pa•s
ρ	mass density, kg/m^3
λ	corrugation pitch, m
Δ	difference
δ	thickness of plate, m
σ	surface tension, N/m

Abbreviations

HFC	hydrofluorocarbon
HFO	hydrofluoroolefin
MAE	mean absolute error
ODP	Ozone Depletion Potential
ORC	organic Rankine cycle
PHE	plate heat exchanger
GWP	Global Warming Potential

1. Introduction

With rising fuel prices and concerns for the environment, utilizing the available energy sources in the most efficient manner and increasing the use of renewable energy sources have become necessities. Low-grade heat is available in different forms, ranging from waste heat including marine diesel engines, industrial processes and refrigeration plants to renewable sources such as biomass combustion, and geothermal and solar heat sources. The organic Rankine cycle (ORC) technology has gained worldwide acceptance as an efficient way to utilise low-grade heat [1] and the ORC market has seen a near exponential growth in the last decade [2]. Due to the large heat transfer area per volume, the plate heat exchanger (PHE) has some great features including compactness, effectiveness, design flexibility and low cost. Plate heat exchangers are the most common type of heat exchangers used in small-scale ORC plants, while shell and tube heat exchangers are commonly used in large-scale ORC systems [2]. Plate heat exchangers can be brazed, gasketed or of shell and plate type. Compared with gasketed and shell and plate heat exchangers, brazed PHEs have better sealing performance, higher resistant to corrosion and pressure load [3]. Brazed PHEs are commonly applied for evaporators in small-scale ORC units [e.g. 4-7], and is therefore the heat exchanger type that is considered in this work. The heat transfer and pressure drop characteristics of organic working fluids in PHEs have significant effects on the ORC design. In this case, the research on the heat transfer and pressure drop performance in PHEs is of crucial importance in order to design heat exchangers for more efficient and economically feasible ORC units.

The accurate evaluation of heat transfer mechanisms during the flow boiling in PHEs is imperative for prediction of the heat transfer coefficient, and thus for the designing

of the heat exchanger. In the flow boiling process, two main heat transfer mechanisms exist, which are named nucleate and convective boiling. A common phenomenon has been presented in some research [8-12], that is, nucleate boiling and convective boiling are predominant at low and high vapour qualities, respectively. With the further increase of vapour quality, the flow enters into the dryout regime. Unlike the experimental results in Refs. [8-12], a nucleate boiling-dominant process was found by Huang et al. [13] when outlet vapour quality x_{out} = 0.4–1. The authors performed an experimental investigation of the heat transfer and pressure drop of R134a and R507A with three industrial PHEs. From the test results, it was concluded that nucleate boiling is dominant in their study, for which the heat transfer coefficient showed a strong dependence on the heat flux, and a weak dependence on the refrigerant mass flux, vapour quality, and the chevron angle. Moreover, Lee et al. [14] carried out an experimental investigation of water flow boiling in the PHE. The results showed that water flow boiling was in the convective boiling region even though the vapour quality and mass flux were relatively low. This phenomenon is different from those reported in Refs. [8-12], and it is attributed to the fact that water has very different thermophysical properties than those of refrigerants. Overall, the issues surrounding which mechanism is predominant for the flow boiling in PHEs and what the proven transition criteria are, remain open.

Furthermore, flow boiling in PHEs is a complex heat transfer process, which is affected by many factors including mass flux, heat flux, vapour quality, saturation temperature (pressure), the properties of the working fluids and the structures of the PHEs. However, experimental results regarding the effects of the above factors on the heat transfer and pressure drop are inconsistent from the open literature. Taking the

effects of saturation temperature on heat transfer as an example, the present results from different research are inconsistent. Khan et al. [11] carried out an experimental investigation of heat transfer and pressure drop of ammonia in a commercial PHE with different saturation temperatures ranging from -25 ℃ to -2 ℃. Experimental results showed a strong influence of saturation temperature and other operational conditions on the heat transfer and pressure drop in the PHE. Both the heat transfer coefficient and pressure drop were found to increase with an increase in saturation temperature. Han et al. [15] conducted the experiments on the evaporative heat transfer and pressure drop in a brazed PHE using refrigerants R410A and R22 and varying the evaporating temperature 5 ℃, 10 ℃ and 15 ℃. From the test results, it can be found that both the evaporation heat transfer coefficient and the pressure drop increase with decreasing evaporation temperature. Longo [16] investigated the effect of heat flux, mass flux, saturation temperature, outlet conditions and fluid properties on heat transfer and pressure drop during HC-600a, HC-290, and HC-1270 flow boiling inside a brazed PHE. The heat transfer coefficients showed weak sensitivity to the saturation temperature ranging from 10 ℃ to 20 ℃ and great sensitivity to heat flux, evaporator outlet condition and fluid properties. Furthermore, in the most recent review for flow boiling and frictional pressure gradients in PHEs [3], the authors claim that compared with single-phase flow inside PHEs which has been widely studied, two-phase flow and heat transfer were studied less. Meanwhile, the authors also emphasize that only a few studies were carried out from different research groups and several empirical correlations have been proposed, but not widely validated beyond their original data set. Thus there are indications that two-phase heat transfer and pressure drop characteristics in PHEs need to be further studied.

In the various experimental and simulation studies of the ORC units, due to the different heat source temperatures and different working fluids, as well as the considerations of different evaluation criteria such as net power output and thermal efficiency, the evaporation temperatures of working fluids have a wide range [1]. For the ORC power systems with heat source temperatures of 100–250 °C, the evaporation temperature is typically in the range 50–150 °C [1, 2]. Nonetheless, the literature survey reveals that most of the experiments were performed under 45 °C and just a few points have been measured at 105 °C [3]. Thus this review indicates an essential lack of experiments with high saturation temperature, corresponding to high reduced pressure, for ORC power system applications. Moreover, combined with the above analysis suggesting that the saturation temperature has significant effects on the flow boiling in PHEs, it can be demonstrated that the experimental investigation of flow boiling with higher saturation temperatures is needed.

Hydrofluorocarbons (HFCs) have the largest share of the current refrigerant market [17], which are with no Ozone Depletion Potential (ODP) but have extremely high Global Warming Potential (GWP). In order to meet the demand of environmental protection, hydrofluoroolefins (HFOs) have been developed as fourth-generation refrigerants with low GWP values [18]. Some studies using HFOs as the working fluid in the ORC units have been conducted to compare with results of conventional HFCs. The results indicated that some HFOs show great potential to replace HFCs as working fluids in the ORC unit. Liu et al. [17] investigated the feasibility of a series of hydrofluoroolefins as potential working fluids for applications in geothermal ORC power generation. From the simulations, it can be found that R1234yf is suitable for the low temperature geothermal ORC power generation (geothermal heat source

temperature is 120 °C), while R1225yeE is very promising for geothermal brine with temperatures around 150 °C. Nevertheless, in terms of heat transfer, there is also a lack of experimental investigations on the flow boiling of HFOs in PHEs. The only study the authors found in the literature with HFOs (R1234yf) in PHEs was performed by Longo and Zilio [19], in which R1234yf condensation experiments with saturation temperature of 25–40 °C were carried out. Their experimental results suggest that HFO1234yf exhibits heat transfer coefficients lower (10–12%) and frictional pressure drop lower (10–20%) than those of HFC134a under the same operating conditions.

The objective of this paper is to obtain the flow boiling heat transfer and pressure drop characteristics of HFOs in PHEs at high saturation temperatures and to develop new correlations for thermal-hydraulic performance as necessary. In order to complete these goals, a series of experiments were conducted at a test facility built at the Technical University of Denmark (DTU). As the working fluid most commonly used in geothermal power plants or in very low temperature water heat recovery [2], HFC R134a was selected as the working fluid, and thus its test results were used as the baseline to compare with those of the two HFO working fluids, R1234yf and R1234ze, which are developed as the replacements for R134a. The heat transfer and pressure drop performances of these three working fluids were measured with three saturation temperatures, 60 °C, 70 °C and 80 °C (the corresponding reduced pressures are presented in Table 1) and different mass fluxes, heat fluxes and vapour qualities. Generally, the experiments were carried out at working conditions which prevail in the evaporator of ORC units.

Table 1 Reduced pressures of working fluids under different saturation temperatures

	60 °C	70 °C	80 °C

R134a	0.41	0.52	0.64
R1234yf	0.48	0.60	0.74
R1234ze	0.35	0.44	0.55

The paper proceeds with a description of the methodology used, including the experimental apparatus and data analysis in Section 2. Then the test results and discussion are presented in Section 3. Finally, conclusions are given in Section 4.

2. Methods

2.1 Experimental apparatus

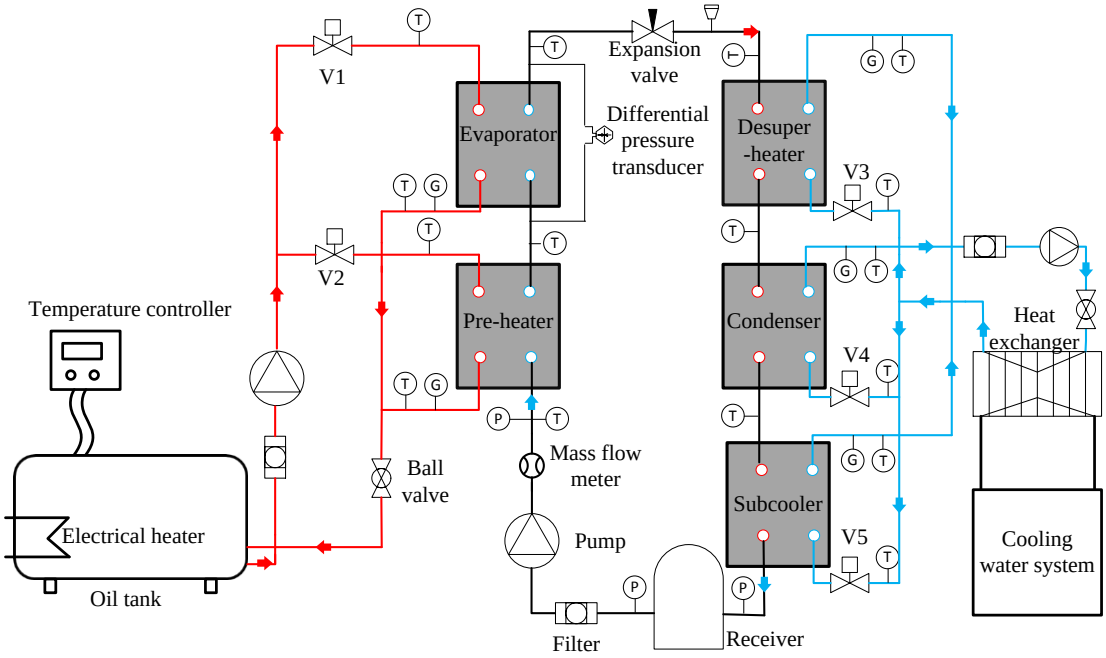

Figure 1 Schematic of the test facility

The experimental system designed for this work is shown schematically in Figure 1, which mainly consists of three fluid loops, one primary working fluid cycle and two auxiliary loops used to evaporate and condense the primary working fluid, respectively. In the main cycle, a variable speed volumetric pump is used to circulate

the working fluid as well as control the mass flow rate. The working fluid is pumped from the receiver through a filter, mass flow meter, pre-heater and evaporator. In the pre-heater, the subcooled working fluid is heated to control the evaporator inlet quality and to ensure that the heat transfer process in the evaporator is only saturated flow boiling without subcooled boiling. In the evaporator, the two-phase working fluid is further heated to reach the required outlet vapour qualities. Thermocouples and differential pressure transducer are installed at the inlet and outlet of the evaporator to measure the temperature and the pressure difference of the working fluid, respectively. The saturation temperature (pressure) in the evaporator is controlled by regulating an expansion valve installed at the outlet of the evaporator. After the expansion, the heated two-phase working fluid flow through three PHEs, the desuperheater, condenser and subcooler in sequence, which are used to desuperheat, condense and subcool the working fluid, and finally it enters the receiver tank for storage.

In the heating loop, an oil based heat transfer fluid is heated in the oil tank by electrical heaters. A temperature controller is connected with the oil tank to enable the simulation of different heat source temperatures. After the oil is heated to the specified temperature, a variable speed volumetric pump are circulating the heating oil to flow through the pre-heater and evaporator in parallel. During all the experiments, the pump speed was changed to regulate the oil mass flow rate and thus control the heat flux transferred from the oil to the working fluid. By this operation, the inlet and outlet vapour qualities of the evaporator could be reached as the setting values. The heat rejection to the cooling water system is obtained by circulation of chilled water in parallel flows for the desuperheater, condenser and subcooler. By

adjusting the mass flow rate and temperature of the chilled water, the condensation pressure of the working fluid is controlled. Moreover, the temperatures, as well as the volume flow rates, of both the heating oil and cooling water are measured at the inlet and outlet of each PHE. Five solenoid valves, V1–V5, are installed at the inlet of the five respective PHEs used to control the mass flow rates of the heating and cooling fluids as necessary.

The plate heat exchanger used as the evaporator (test section) in the test rig is a commercial brazed PHE with compact structure. It has 10 plates in total, 5 oil passes and 4 working fluid passes. The total heat transfer area is 0.186 m^2. Figure 2 shows the schematic of a chevron-type plate, and the main dimensions of the current stainless plate (which were measured) are listed in Table 2.

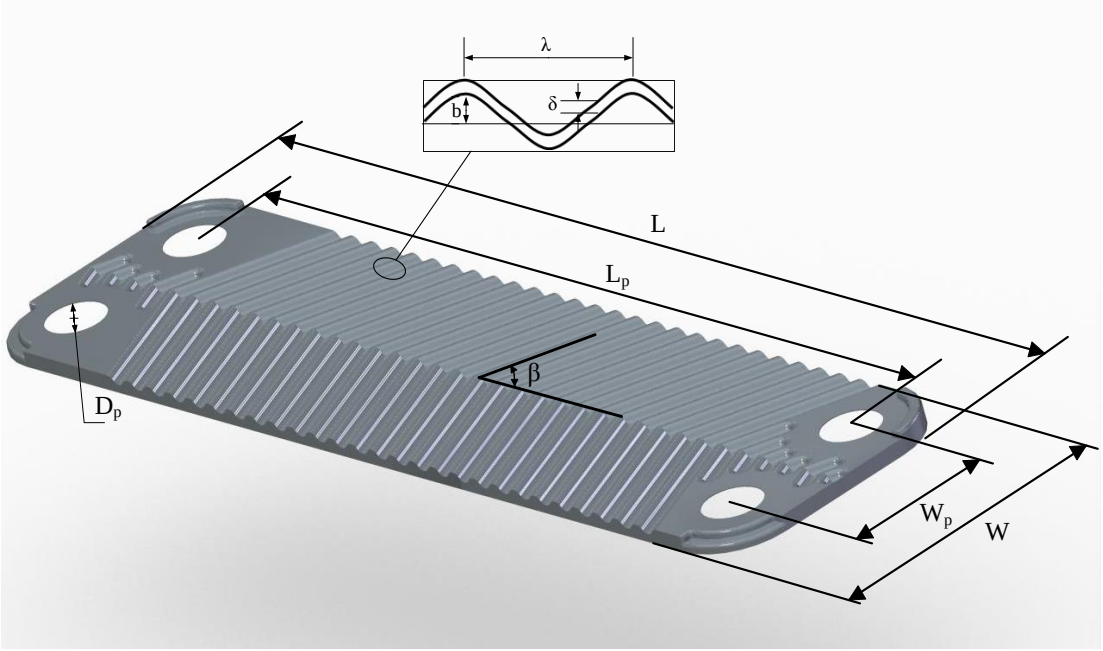

Figure 2 Schematic of a chevron-type plate

Table 2 Geometrical data of the chevron plate

Parameters	Measured values

Length L (mm)	317
Width W (mm)	76
Port-to-port length L_p (mm)	278
Port-to-port width W_p (mm)	40
Diameter of inlet/outlet port D_p (mm)	36
Chevron angle β (°)	65
Corrugation pitch λ (mm)	7
Amplitude of corrugation b (mm)	1
Hydraulic diameter D_h (mm) (see the definition in Sec. 2.2.1)	3.4

2.2 Data analysis

2.2.1 Data Reduction

The geometric calculations of the chevron-type plates follow the definitions by Martin [20]. The hydraulic diameter of the working fluid channel between two chevron-type plates D_h is defined as

$$D_h = \frac{4b}{\varphi} \ , \tag{1}$$

where the dimensionless parameter φ is the area enlargement factor caused by sinusoidal surface waviness and calculated by

$$\varphi = \frac{1}{6}(1 + \sqrt{1+\gamma^2} + 4\sqrt{1+\gamma^2/2}) \ , \tag{2}$$

where γ is a dimensionless corrugation parameter, defined as

$$\gamma = \frac{2\pi b}{\lambda} \ . \tag{3}$$

The flow boiling heat transfer coefficient of the working fluid side h_{tf} is determined from

$$\frac{1}{h_{tf}} = \frac{1}{U} - \frac{1}{h_{oil}} - \frac{t_{wall}}{k_{wall}} \ , \tag{4}$$

where the heat transfer coefficient of oil h_{oil} is calculated using Eq. (7), and t_{wall} and

k_{wall} are the thickness and thermal conductivity of the plate, respectively. The overall heat transfer coefficient U of the PHE is computed using the log mean temperature difference (LMTD) method:

$$U = \frac{c_{p,oil}\,\dot{m}_{oil}\,(T_{oil,in}-T_{oil,out})}{A_{eva}\,LMTD} \quad , \tag{5}$$

where the LMTD is calculated as

$$LMTD = \frac{(T_{oil,in}-T_{oil,out})}{\ln(\frac{T_{oil,in}-T_{sat}}{T_{oil,out}-T_{sat}})} \quad , \tag{6}$$

where $T_{oil,in}$ and $T_{oil,out}$ are evaporator inlet and outlet temperatures of oil side, respectively, T_{sat} is saturation temperature in the evaporator, A_{eva} is heat transfer area of evaporator, and $c_{p,oil}$ and $\dot{m}_{oil}$ are specific heat and mass flow rate of oil, respectively.

In order to obtain the h_{oil}, the modified Briggs and Young Wilson plot method [21] for single-phase convective heat transfer was performed using an identical oil/water PHE. The resulting correlation for oil side Nusselt number Nu_{oil} is

$$Nu_{oil} = 0.283 {Re_{oil}}^{0.8} {Pr_{oil}}^{\frac{1}{3}} (\mu_{wall}/\mu_{oil})^{0.14} \quad , \tag{7}$$

where Re_{oil} and Pr_{oil} are Reynolds number and Prandtl number of oil respectively, and μ_{oil} and μ_{wall} are dynamic viscosities based on mean oil temperature and wall temperature, respectively.

The refrigerant quality at the inlet of the evaporator x_{in} may be calculated by [15]

$$x_{in} = \frac{1}{h_{fg}}\left[\frac{\dot{Q}_{pre}}{\dot{m}_{wf}} - c_{p,f}\left(T_{sat} - T_{wf,pre,in}\right)\right] \quad , \tag{8}$$

where h_{fg} is enthalpy of evaporation, $\dot{Q}_{pre}$ is the heat transfer rate of evaporator, $c_{p,f}$ and $\dot{m}_{wf}$ are specific heat and mass flow rate of working fluid respectively, and

$T_{wf,pre,in}$ is the pre-heater inlet temperature in the working fluid side.

The vapour quality difference between the inlet and outlet of the evaporator Δx is given by

$$\Delta x = x_{out} - x_{in} = \frac{qA_{eva}}{h_{fg}\dot{m}_{wf}} \ , \tag{9}$$

where q is heat flux in the evaporator.

The measured pressure difference of the two-phase flow between the inlet and outlet of the evaporator includes the static (gravitational) ΔP_g, acceleration ΔP_{acc}, the total frictional pressure drops across PHE ΔP_{fri}, and the pressure drops across the inlet and outlet ports ΔP_p. Therefore, the total frictional pressure drops across the PHE is given by

$$\Delta P_{fri} = \Delta P_{tot} - \Delta P_p - \Delta P_g - \Delta P_{acc} \ . \tag{10}$$

The port pressure drop ΔP_p is obtained by

$$\Delta P_p = 0.75 \frac{G_p^2}{\rho_m} \ , \tag{11}$$

where the G_p is working fluid mass flow rate based on the flow area of plate port. The average two-phase density between the inlet and outlet of the PHE ρ_m is calculated at the average vapour quality between the inlet and outlet x_m

$$\frac{1}{\rho_m} = \frac{x_m}{\rho_v} + \frac{1-x_m}{\rho_l} \tag{12}$$

$$x_m = \frac{(x_{out}+x_{in})}{2} \ , \tag{13}$$

where ρ_l and ρ_v are the densities of liquid-phase and vapour-phase, respectively.

The gravitational and acceleration pressure losses may be evaluated theoretically by

the homogeneous model, which gives

$$\Delta P_g = \rho_m g L_p \tag{14}$$

$$\Delta P_{acc} = G_{wf}^2 \Delta x (\frac{1}{\rho_v} - \frac{1}{\rho_l}) , \tag{15}$$

where G_{wf} is working fluid mass flow rate based on the flow area between two plates.

After obtaining the value of ΔP_{fri}, the two-phase Fanning friction factor f_{tp} can be determined from

$$\Delta P_{fri} = 2 f_{tp} \frac{L_p G_{wf}^2}{D_h \rho_m} \quad . \tag{16}$$

2.2.2 Uncertainties analysis

In this study, the temperature measurement uncertainty was ± 0.19 K. The errors associated with the mass flow rate and volume flow rate were ± 0.015 % and ± 0.5 %, respectively. The pressure and pressure difference uncertainties were ± 0.45 % FS (Full Span of 5 MPa) and ± 0.046 %, respectively. All uncertainty figures were provided by the manufacturer of the measuring devices. The uncertainties of the parameters which are calculated by directly measured values, such as the friction factor f_{tp}, the inlet and outlet qualities x_{in} and x_{out}, the heat flux q and the heat transfer coefficient h_{tp} are generally denoted as z and described as follows:

$$z = f(y_1, y_2, \dots \dots y_n) \tag{17}$$

$$\delta z = \sqrt{\left[\left(\frac{\partial z}{\partial y_1}\delta y_1\right)^2 + \left(\frac{\partial z}{\partial y_2}\delta y_2\right)^2 \dots \dots + \left(\frac{\partial z}{\partial y_n}\delta y_n\right)^2\right]} , \tag{18}$$

where δy_1, δy_2, …… δy_n, are the directly measured value uncertainties. The ranges of the uncertainties of the main parameters are reported in Table 3.

Table 3 Uncertainty in operating conditions

	Value	Uncertainty		Value	Uncertainty
x_{out}	0.5 – 0.99	0.9 % – 2.1 %	q (kW/m^2)	9.8 – 36.8	1.3 % – 2.8 %
ΔP_{fri} (kPa)	0.02 – 22.7	1.3 % – 6.6 %	h_{wf} (W/m^{2}K)	3258 – 7983	3.5 % – 12.8 %
f_{tp}	0.03 – 0.75	3.3 % – 8.4 %	Nu_{tp}	177 – 570	4.1 % – 15.6 %

3. Results and discussion

In this study, three working fluids were tested at the same working conditions which included outlet vapour qualities, mass fluxes, heat fluxes and saturation temperatures, which ranged from 0.5 to 1, 86 kg/m^{2}s to 137 kg/m^{2}s, 9.8 kW/m^2 to 29.6 kW/m^2, 60 °C to 80 °C, respectively. Across all measurements, due to the changes of heat fluxes brought by the oil, the working fluids' inlet vapour qualities of the evaporator maintained the value of 0.1 – 0.3. The larger inlet vapour qualities correspond to the larger outlet vapour qualities.

3.1 Experimental validation

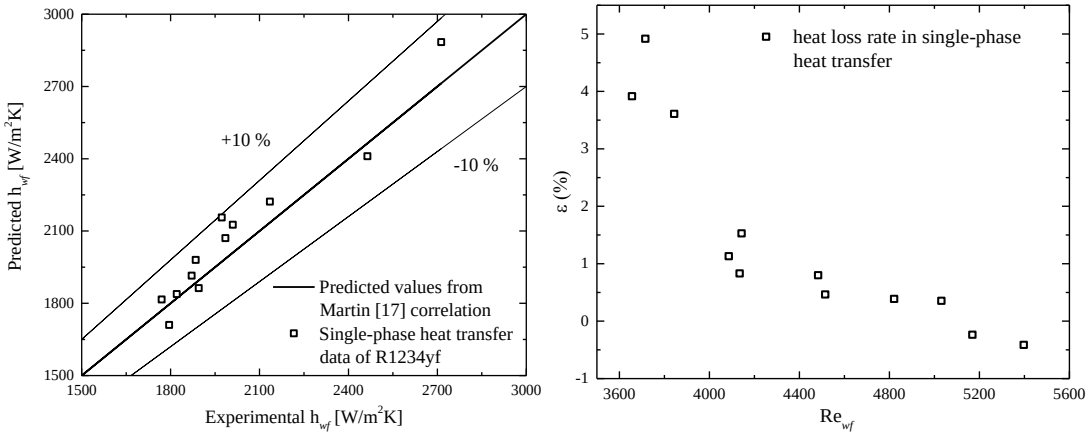

(a) (b)

Figure 3 (a) Comparison of the present single-phase R1234yf convection heat transfer data with the correlation from Martin [20]. (b) Heat loss rate in single-phase heat transfer.

In order to validate the test facility, single-phase heat transfer experiments using R1234yf as the working fluid were performed and the results were compared with the existing PHE prediction methods of single-phase heat transfer. Figure 3(a) compares the experimental results with the predicted values from the well-known Martin correlation [20], suggesting that the measured results fall within ±10 % of the Martin correlation [20]. The results indicate that the test facility is accurate for the single-phase heat transfer, and hence can be expected to be accurate also for two-phase heat transfer.

Moreover, the heat loss rates in the single-phase heat transfer experiments are plotted as the function of the R1234yf Reynolds number in Figure 3(b), which is defined as

$$\varepsilon = \frac{c_{p,wf}\,\dot{m}_{wf}\,(T_{wf,out}-T_{wf,in})-c_{p,oil}\,\dot{m}_{oil}\,(T_{oil,in}-T_{oil,out})}{c_{p,oil}\,\dot{m}_{oil}\,(T_{oil,in}-T_{oil,out})}\,100\ \%\ , \qquad (19)$$

where $c_{p,oil}$ is the specific heat of working fluid and $T_{wf,in}$ and $T_{wf,out}$ are inlet and outlet temperatures of working fluid side, respectively. As shown in Figure 3(b), the heat loss rate is less than 5 % with the working fluid Reynolds number ranging from 3600 to 5500. Moreover, as indicated in the figure, the heat loss rate decreases with the working fluid Reynolds number. The same trend applies to the heat transfer rate. Therefore, in the two-phase heat transfer for which the heat transfer rate is higher than that in single-phase flow, the heat loss rate is expected to be less than 5 %, suggesting that the measurements taken in the study are accurate.

3.2 Heat transfer

Figure 4 shows the heat transfer coefficient variation of the three working fluids as a function of heat flux at various mass fluxes and saturation temperatures. As shown in Figure 4, the heat transfer coefficients of each working fluid at the same saturation

temperature are strongly dependent on the heat flux. Specifically, most of the heat transfer coefficients are the power function of the heat flux except for some declining points, which suggests that dryout occurred. The dryout phenomenon will be discussed in the following section. The power function followed by the heat transfer coefficient and heat flux can be defined as

$$h = Cq^n. \tag{20}$$

As noted in Ref. [22], the characteristic of the h – q curves expressed by Eq. (20) can be obtained for all substances in the nucleate boiling regime.

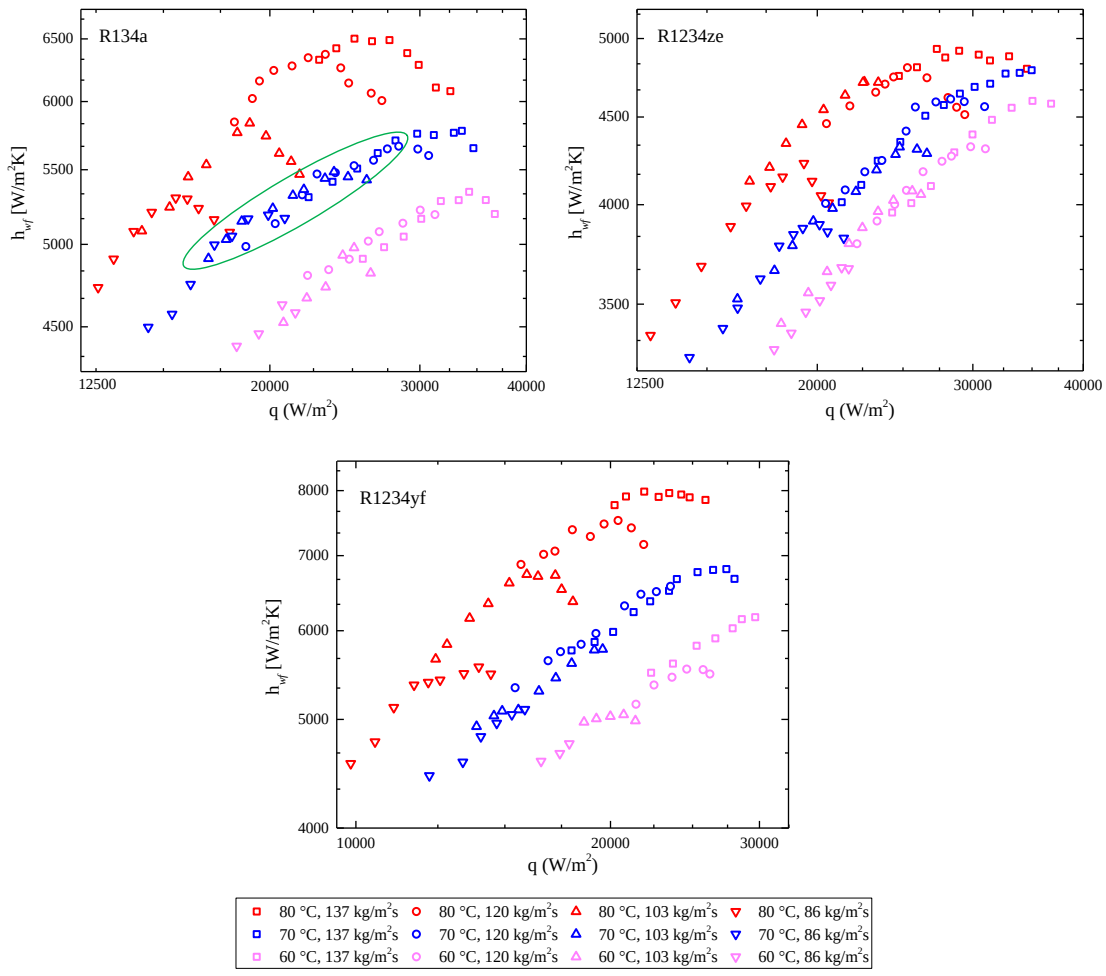

Figure 4 Heat transfer coefficients of the three working fluids as a function of heat flux with different mass fluxes and saturation temperatures

Figure 4 also suggests that the heat transfer coefficient is affected by the mass flux to some extent. Taking the working condition of R134a at T_{sat} = 70 °C as an example, some test points were measured at the same heat flux but different mass flux, which are involved in the area of the green circle. Comparing the data in this area, heat transfer coefficients are weakly sensitive to the mass flux. This phenomenon can also be found in the other working conditions with different working fluids and saturation temperatures.

In order to study further the dominant heat transfer regime during the flow boiling in the PHE, the Thonon et al. [23] criterion was used in this study. This criterion estimates the transition line between the nucleate and the convective boiling regions using the product of the Lockhart-Martinelli parameter (X_{tt}) and boiling number (Bo), defined as

$$Bo = \frac{q}{Gi_{fg}} \tag{21}$$

$$X_{tt} = (\frac{1-x_m}{x_m})^{0.9}(\frac{\rho_v}{\rho_l})^{0.5}(\frac{\mu_l}{\mu_v})^{0.1}\ , \tag{22}$$

where μ_l and μ_v are working fluids dynamic viscosities of liquid-phase and vapour-phase, respectively. As $X_{tt} \cdot Bo > 0.00015$, nucleate boiling is dominant, while $X_{tt} \cdot Bo < 0.00015$, convective boiling is dominant. As shown in Figure 5, all the data belong to the nucleate boiling region.

The results of the experimental analysis suggest that the heat transfer coefficient is strongly dependent on heat flux and weakly dependent on mass flux. This conclusion as well as the Thonon et al. [23] criterion, indicate that nucleate boiling is the dominant heat transfer regime in this study. However, the working conditions in this study including heat flux, mass flux and vapour quality are not completely

independent; they are correlated with each other. As summarized by Thome [24], the interrelation between the effects of heat flux, mass flux and vapour quality on flow boiling are very strong, making the interpretation of experimental trends particularly challenging. More experiments with independent working conditions need to be performed in order to verify the conclusion about the heat transfer regime.

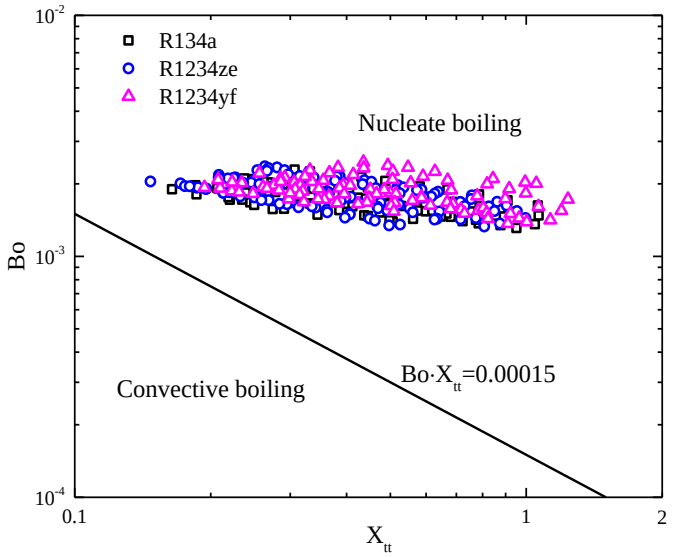

Figure 5 Experimental data in this study based on the Thonon et al. [24] criterion

As mentioned above, it can be found that in Figure 4, the heat transfer coefficients will decrease with the further increase of heat flux. This phenomenon may be attributed to the fact that dryout was triggered under the condition where the heat flux exceeded the critical heat flux (CHF) and thus the heat transfer entered the liquid deficient region [24]. It is important to note that the CHF used in the flow boiling should not be confused with the same terminology in the pool boiling. In the latter case, the CHF indicates the failure of the heat transfer surface, termed physical burnout, while the CHF in the former case means that deterioration of the heat transfer process in the evaporator occurs [24,25]. Moreover, the phenomenon that dryout is

triggered with the increase of heat flux resulting in the decrease of the heat transfer coefficient, is most remarkable at the highest saturation temperature of 80 °C. As noted by Thome [24], the CHF decreases with increasing pressure and increases with increasing mass flux. This conclusion suggests that lower CHF occurs at the higher saturation temperature, facilitating and more frequently triggering dryout, and thereby the heat transfer coefficient decreases more sharply at the higher saturation temperature.

The above experimental analysis suggests that the nucleate boiling regime is dominant even though vapour qualities were relatively high in this study. Figure 6 exemplifies the heat transfer coefficient as a function of mean vapour quality for R134a at T_{sat} = 70 °C. It can be observed that the nucleate boiling is dominant until x_m > 0.5, since this is the point where the heat transfer coefficient becomes more or less independent of the heat flux. Similar trends can also be found in all other working conditions. Compared with the experimental results in Refs. [8-12], the vapour quality corresponding to the nucleate-convective boiling transition in this study is larger, which indicates that nucleate boiling is more difficult to be suppressed under the working conditions in this study.

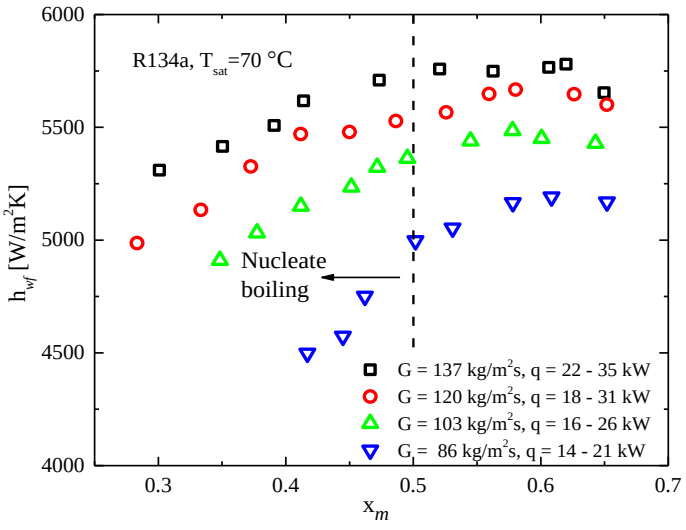

Figure 6 Heat transfer coefficient of R134a as a function of mean vapour quality at T_{sat} = 70 °C and G = 86 kg/m^{2}s – 137 kg/m^{2}s

The difference may be attributed to the effect of the saturation temperature/pressure on the heat transfer, indicating that the nucleation of bubbles becomes easier at higher saturation temperatures. Specifically, with the increase of saturation temperature/pressure, the surface tension σ decreases and the slope of the equilibrium vapour pressure curve $(dP/dT)_{sat}$ increases, both contributing to increasing the number of active nucleation sites [22]. Moreover, conventional nucleation theory states that the required wall superheat for the nucleation of bubbles becomes greater as pressure decreases [26]. Ross et al. [27] observed a complete suppression of nucleate boiling with R152b at low pressures, while nucleate boiling was not suppressed at higher pressures. Besides, from the sight of bubble behavior, it can be found that the bubble departure diameter decreases and the bubble departure frequency increases with the increasing saturation pressure [28]. This yields more intense evaporation and promotes turbulence in the near-wall region, thus enhancing heat transfer. The above analysis about the effect of saturation temperatures on heat transfer also explains the experimental results shown in Figure 4; heat transfer coefficients increase with increasing saturation temperatures/pressure for each working fluid. In order to quantify the effects of saturation temperature on thermo-physical properties and heat transfer, the changes of $(dP/dT)_{sat}$, σ and h_{tf} for three working fluids under different saturation temperatures is presented in Table 4. The thermo-physical properties $(dP/dT)_{sat}$ and σ are selected because these are two important parameters that affect nucleate dominant heat transfer processes. As shown in Table 4, R1234yf has a maximum h_{tf} average increase of 24 %, as the temperature rise from 60 °C to 80 °C,

as a consequence of an increase of 39 % in $(dP/dT)_{sat}$ and decrease of 70 % in σ, respectively.

Table 4 Change of $(dP/dT)_{sat}$, σ and average h_{tf} at T_{sat} = 70 °C and 80 °C compared with those at T_{sat} = 60 °C

	80 °C			70 °C		
	$(dP/dT)_{sat}$	σ (mN/m)	h_{tf} (W/m^2 K)	$(dP/dT)_{sat}$	σ (mN/m)	h_{tf} (W/m^2 K)
R134a	+41 %	-57 %	+17 %	+19 %	30 %	+8 %
R1234yf	+39 %	-70 %	+24 %	+18 %	-35 %	+9 %
R1234ze	+41 %	-48 %	+12 %	+19 %	-24 %	+5 %

From Figure 4, it can be further found that at the same saturation temperature, R1234yf and R1234ze have the highest and lowest heat transfer coefficients, corresponding to the order of reduced pressure values listed in Table 1. In order to identify the effect of the working fluid properties on heat transfer, some test data are selected and compared in the following. Due to the relatively close reduced pressure values, the heat transfer coefficients under the working conditions of R134a at 80 °C and R1234yf at 70 °C, and R134a at 70 °C and R1234ze at 80 °C, are compared in Figures 7(a) and (b), respectively. Specifically, the reduced pressures of R134a at 80 °C and R1234yf at 70 °C are 0.64 and 0.60, giving a relative error of 6.3 % in reduced pressures, while the reduced pressures of R134a at 70 °C and R1234ze at 80 °C are 0.52 and 0.55, giving a relative error of 5.4 % in reduced pressures. The reduced pressure in each group can be considered approximately equivalent. Comparing the experimental results in Figure 7, the heat transfer coefficients of R134a and R1234yf do not have a significant difference when ignoring the test data in the saturated dryout region, meanwhile the heat transfer coefficients of R134a are on

average 20 % higher than those of R1234ze.

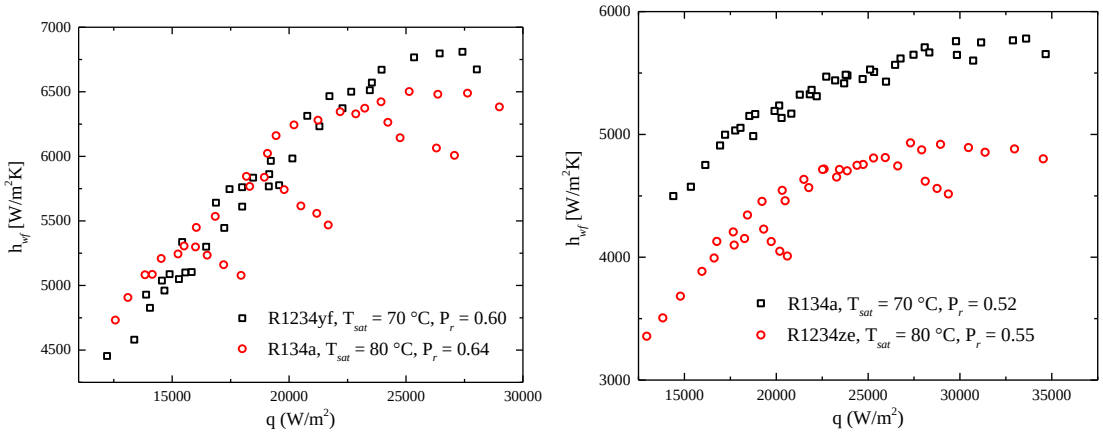

(a) (b)

Figure 7 Comparison of heat transfer coefficients for (a) R134a, T_{sat} = 80 °C, P_r = 0.64 and R1234yf, T_{sat} = 70 °C, P_r =0.60 (b) R134a, T_{sat} = 70 °C, P_r = 0.52 and R1234ze, T_{sat} = 80 °C, P_r =0.55

4.3 Pressure drop

Figure 8 depicts the frictional pressure drop variation of the three working fluids as a function of the outlet vapour quality with different mass fluxes and saturation temperatures. From Figure 8, it can be found that the frictional pressure drop increases with the increase of vapour quality and mass flux. The acceleration of the flow caused by the higher vapour quality and mass flux, results in a steeper velocity profile at the channel wall, which contributes to the higher pressure drop.

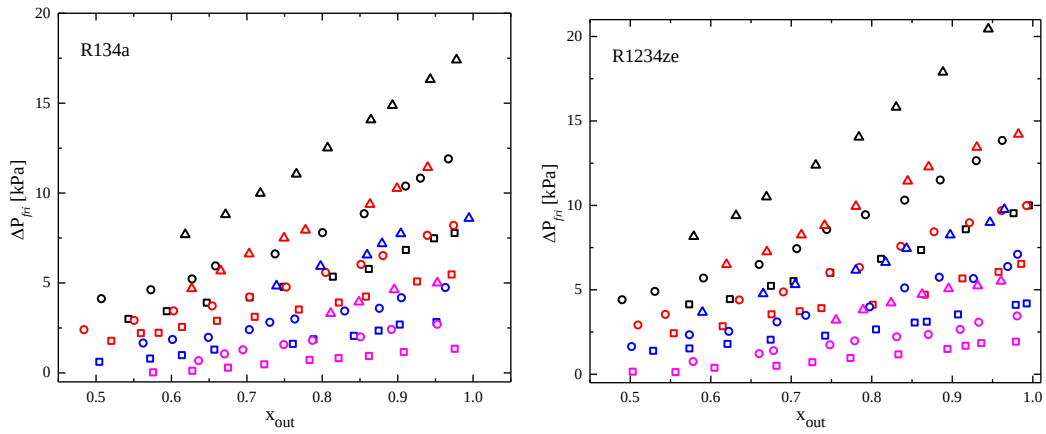

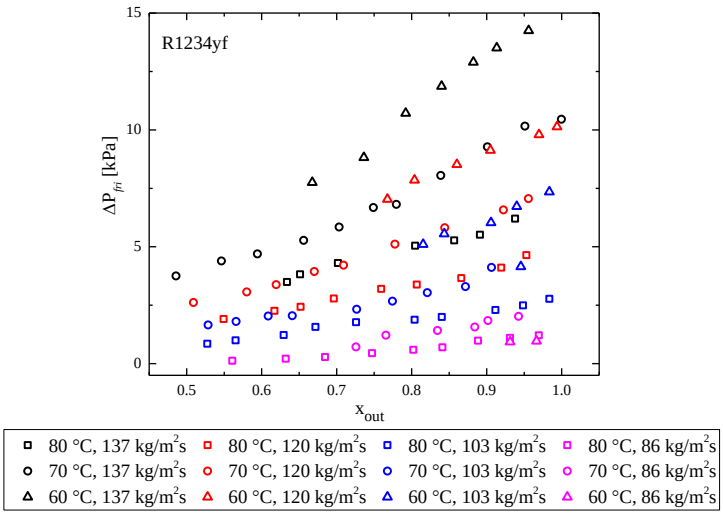

Figure 8 Frictional pressure drops of three working fluids as a function of vapour quality with different mass fluxes and saturation temperatures

From Figure 8, it can be further found that the frictional pressure drop increases with the decrease of the saturation temperature. This is attributed to the fact that the density difference between the liquid and vapour increase due to the decrease of the saturation temperature, and thus the velocity difference between the liquid and vapour phases increases. In this case, the shear stress at the liquid–vapour interface increases, resulting in the higher frictional pressure drop.

The analysis about the effect of the liquid–vapour density difference on the pressure drop is also suitable for the effect of different working fluids on pressure drops. At the same saturation temperature, the three working fluids have different liquid–vapour density differences, and the order is (in descending order) R1234ze, R134a and R1234yf. The comparisons of the frictional pressure drop for the three working fluids are presented in Figure 9. As can be seen, R1234ze has the highest frictional pressure drop, while the pressure drop of R1234yf is the lowest, which is consistent with the order of the liquid–vapour density difference. Combined with the experimental results

of the heat transfer coefficients, in terms of the thermal-hydraulic performance in a plate heat exchanger, R1234yf is indicated as a suitable replacement for R134a due to the higher heat transfer coefficient and lower pressure drop. Conversely, R1234ze is not suggested for use as the substitute for R134a within the current operational conditions.

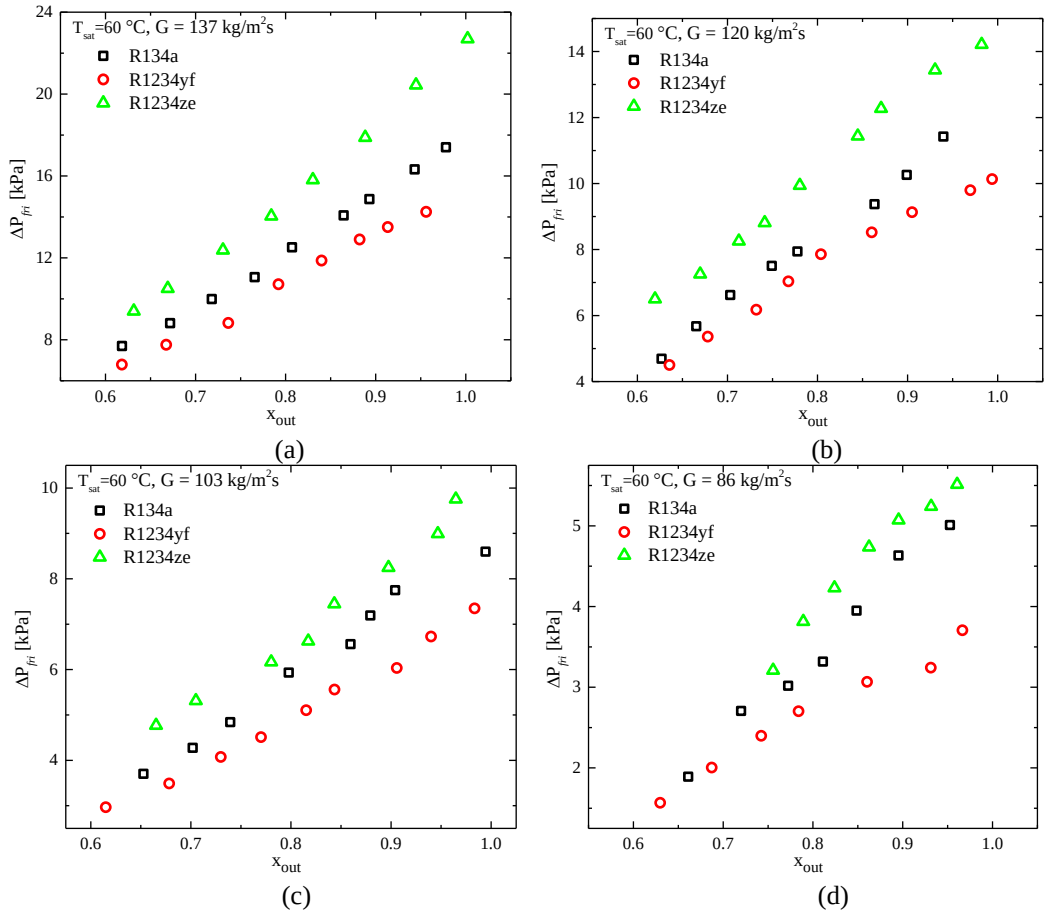

Figure 9 Comparison of frictional pressure drops for different working fluids at G = (a) 137 kg/m^{2}s, (b) 120 kg/m^{2}s, (c) 103 kg/m^{2}s and (d) 86 kg/m^{2}s

4. 3 Two-phase flow boiling correlations

The present correlations obtained by other researchers were deduced based on experimental data obtained at low saturation temperatures, and none of those were deduced for HFOs as working fluids. In order to verify some existing prediction methods, the experimental results obtained in this study are compared with the

predicted values of a few correlations. Table 5 summarizes the equations and experimental conditions in each study. The correlations by Amalfi et al. [29] were developed from an experimental databank for plate heat exchangers including 1903 heat transfer data and 1513 pressure drop data published by thirteen research groups in the literature. The correlations by Huang et al. [13] and Cooper [30] are selected because they are applicable for nucleate boiling. Moreover, the rest of the correlations have been assessed by Amalfi et al. [29] using separate comparisons of the experimental data of each individual research group and showing the best agreements between the predicted and the experimental evaporation heat transfer.

Table 5 Summary of correlations for flow boiling heat transfer and pressure drop in plate heat exchangers

Reference	Correlation	Condition
Huang et al. [13]	$Nu_{tp} = 1.87 \times 10^3 (\frac{qd_0}{k_l T_{sat}})^{0.56} (\frac{i_{fg} d_0}{\alpha_l^2})^{0.31} Pr_l^{0.33}$ $d_0 = 0.0146\theta[\frac{2\sigma}{g(\rho_l - \rho_v)}]^{0.5}, \theta = 35°, \alpha = \frac{k_l}{\rho_l c_{pl}}$	R134a and R507A, b = 2 mm, λ = 8.1 mm, β =28°, 60° and 28°/60°, G = 4 kg/m^{2}s - 32 kg/m^{2}s
Thonon et al. [23]	$\phi_l^2 = 1 + \frac{C}{X} + \frac{1}{X^2}, \phi_l^2 = \frac{\Delta P_{tf}}{\Delta P_l}, X^2 = \frac{\Delta P_l}{\Delta P_v}$	C = 12, single phase pressure drop ΔP_l and ΔP_v are calculated by Martin correlation [16]
Amalfi et al. [29]	$Bd < 4, Nu_{tp} = 982\beta^{*1.101} We_m^{0.315} Bo^{0.32} \rho^{*-0.224}$ $Bd \geq 4, Nu_{tp} = 982\beta^{*1.101} Re_v^{0.135} Re_{lo}^{0.351} Bd^{0.235} Bo^{0.198} \rho^{*-0.224}$ $, \beta^* = \frac{\beta}{\beta_{max}}, \rho^* = \frac{\rho_l}{\rho_v}, Re_v = \frac{G x_m D_h}{\mu_v}, We_m = \frac{G^2 D_h}{\rho_m \sigma},$ $Bd = \frac{(\rho_l - \rho_v) g D_h^2}{\sigma}$	1930 heat transfer data and 1513 frictional pressure drop published by 13 research groups
Cooper [30]	$h_{tp} = 35 P_r^{0.12} (-\log_{10} P_r)^{-0.55} M^{-0.5} q^{0.67}$	Nucleate boiling, 250 points for water in vertical tubes with pressure ranging from 0.25 bar to 71 bar
Donowski and Kandlikar	$h_{tp} = 1.055(1.056Co^{-0.4} + 1.02Bo^{0.9}) x_m^{-0.12} h_{lo}^{0.98}$ $Co = (\frac{\rho_v}{\rho_l})^{0.5} (\frac{1 - x_m}{x_m})^{0.8}, = \frac{q}{G i_{fg}}, Re_{lo} = \frac{G D_h}{\mu_l}$	Based on the test data in Ref. [31]

[31]	$h_{lo} = 0.2121 Re_{lo}^{0.78} Pr_l^{\frac{1}{3}} \left(\frac{\mu}{\mu_{wall}}\right)^{0.14} \left(\frac{k_l}{D_h}\right)$	
Park and Kim [32]	$f_{tp} = 2.478 \cdot 10^7 Re_{eq}^{-1.566} Re_{lo}^{-0.5}, Re_{eq} < 6000$ $f_{tp} = 3.561 \cdot 10^3 Re_{eq}^{-0.532} Re_{lo}^{-0.5}, Re_{eq} \geq 6000$	R134a, D_h = 5.6 mm, β = 45°
Hsieh and Lin [33]	$f_{tp} = 61000 Re_{eq}^{-1.25}$ $Re_{eq} = \frac{G_{eq} D_h}{\mu_l}$, $G_{eq} = G[1 - x_m + x_m(\frac{\rho_l}{\rho_v})^{0.5}]$	R410A, b = 3.3 mm, λ = 10 mm, β =60°, G = 50 kg/m^{2}s - 125 kg/m^{2}s, T_{sat} = 10 °C – 20 °C
Yan and Lin [34]	$f_{tp} = 6.947 \cdot 10^5 Re_{eq}^{-1.109} Re_{lo}^{-0.5}, Re_{eq} < 6000$ $f_{tp} = 31.21 Re_{eq}^{0.04557} Re_{lo}^{-0.5}, Re_{eq} \geq 6000$	R134a, b = 3.3 mm, λ = 10 mm, β =60°,

Figure 10 depicts the comparisons of experimental values and predicted values using the correlations in Table 5 for heat transfer coefficients. The method by Cooper [30] provides reasonable agreement with most of the experiment data within ±30 % error, but it overestimates the data in the dryout region, while the other three correlations cannot predict the experimental results or tendencies well.

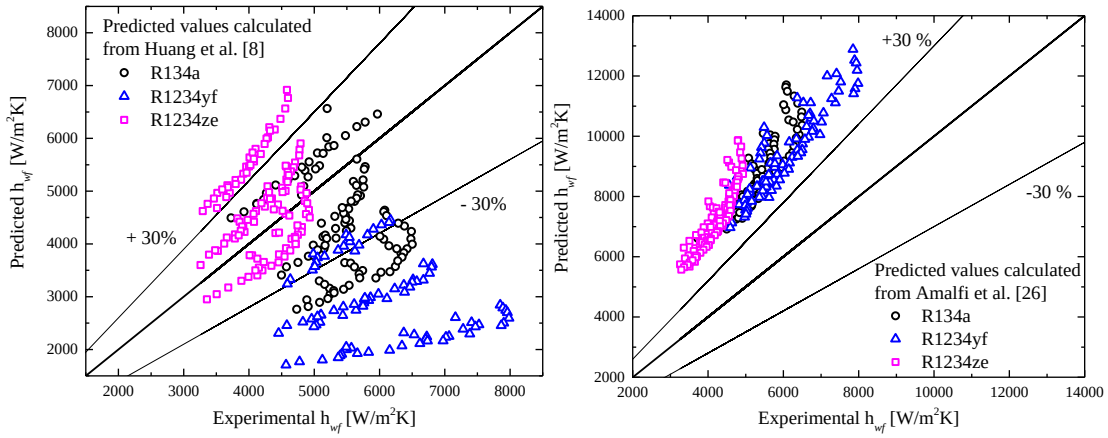

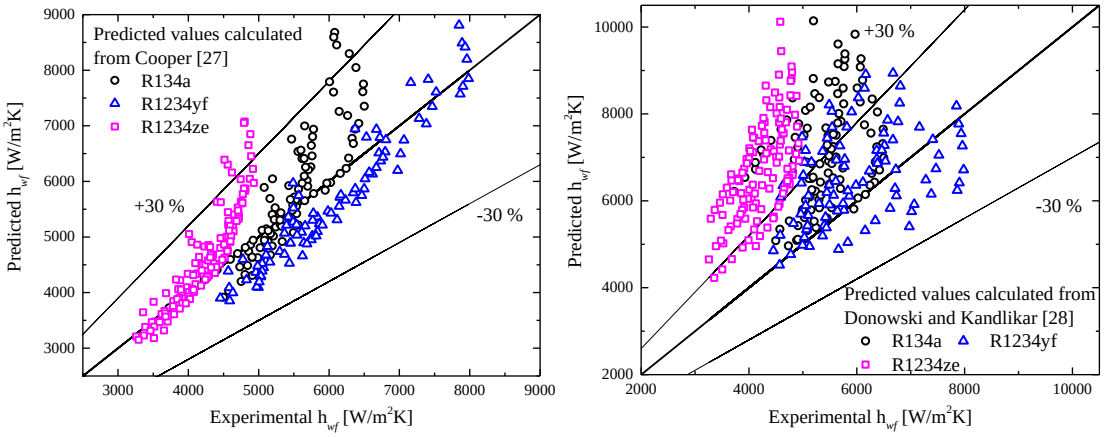

Figure 10 Predicted flow boiling heat transfer coefficients against experimental heat transfer coefficients using different correlations

A new heat transfer correlation is developed based on the data obtained in this paper using linear interpolation of the nucleate boiling and dryout contributions. It is defined as

$$h_{tp} = \frac{x_{cri}-x_{in}}{x_{out}-x_{in}} h_{Cooper} + \frac{x_{out}-x_{cri}}{x_{out}-x_{in}} h_v \,, \tag{23}$$

where h_v and h_{Cooper} are given by the Dittus-Boelter [35] and Cooper [30] correlations to express the heat transfer process in the dryout region and the nucleate boiling dominant region, respectively, defined as

$$h_v = 0.023 Re_v^{0.8} Pr_v^{0.4} \frac{k_v}{D_h} \tag{24}$$

$$h_{cooper} = 35 P_r^{0.12} (-\log_{10} P_r)^{-0.55} M^{-0.5} q^{0.67} \,. \tag{25}$$

A "critical" vapour quality x_{cri} is introduced to calculate the percentages of the nucleate boiling and dryout in the whole heat transfer process. For each working condition, the corresponding "critical" vapour quality x_{cri} is defined as

$$x_{cri} = \begin{cases} x_{out}, & x_{out} < x_{di} \\ x_{di}, & x_{out} \geq x_{di} \end{cases} \,, \tag{26}$$

where the dryout inception quality x_{di} is developed based on the regressed model by Mori et al. [36], defined as

$$x_{di} = 0.58 * \exp\left[0.54 - 8.513 \times 10^{6} \cdot We_v^{-2.3644} Fr_v^{3.2282} \left(\frac{\rho_v}{\rho_l}\right)^{7.8831}\right] , \quad (27)$$

where Fr_v and We_v are the vapour Froude number and the vapour Weber number, calculated as

$$Fr_v = \frac{G^2}{g\rho_v^2 D_h} \quad (28)$$

$$We_v = \frac{G^2 D_h}{g\rho_v \sigma} . \quad (29)$$

The mean absolute error (MAE), which is used to estimate the error of correlations with respect to the experimental data, is defined as

$$MAE = \frac{1}{n}\sum_{i=1}^{n}\left|\frac{data_{i,exp} - data_{i,pred}}{data_{i,exp}}\right| \times 100\ \%\ , \quad (30)$$

where n is the total number of data points. Figure 11 shows the comparison between the measured and predicted values for the heat transfer coefficients as well as the MAE. From the figure, it can be found that the experimental data of heat transfer fall within ±15%.

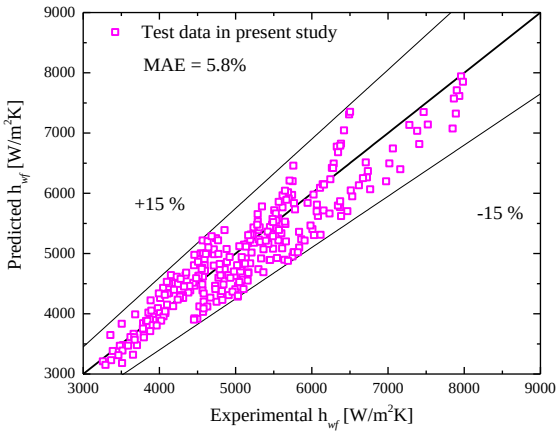

Figure 11 Comparison of proposed correlation (Eq. [23]) with present experimental data for heat transfer coefficients

Figure 12 depicts the comparisons of experimental values and predicted values using the correlations in Table 5 for the pressure drop gradient. As shown in the figure, compared with other correlations, the Yan and Lin [34] method provided the best

predictions for the experimental pressure drop gradient in this study. Based on this fact, a new pressure drop correlation was developed from the correlation by Yan and Lin [34] using the least square method:

$$f_{tp} = \begin{cases} 0.2090 Re_{eq}^{0.6043} Re_{lo}^{-0.5}, & Re_{eq} > 6000 \\ 0.0672 Re_{eq}^{0.7279} Re_{lo}^{-0.5}, & Re_{eq} < 6000 \end{cases}. \quad (31)$$

The comparison between the measured and predicted values for the Fanning friction factor is shown in Figure 13.

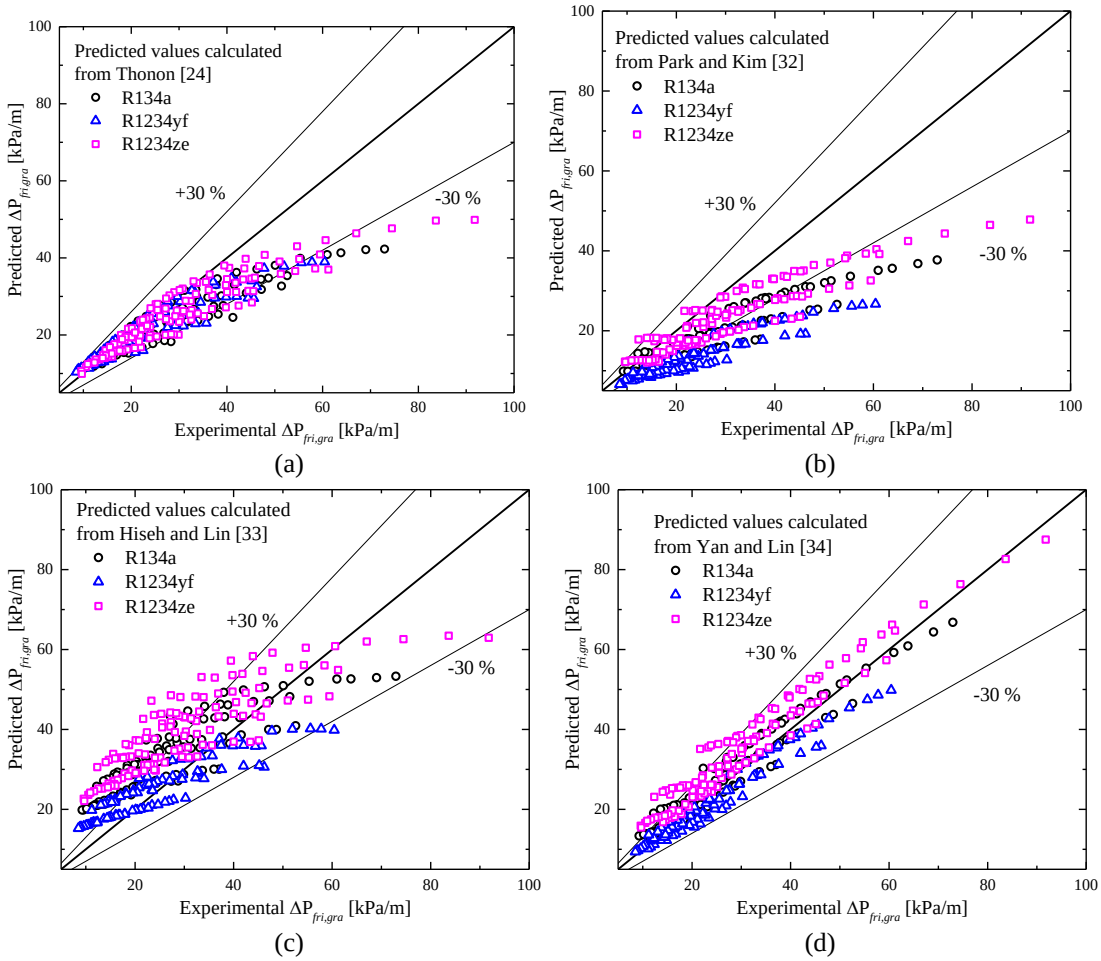

Figure 12 Predicted flow boiling pressure drop gradient against experimental heat transfer coefficients using different correlations

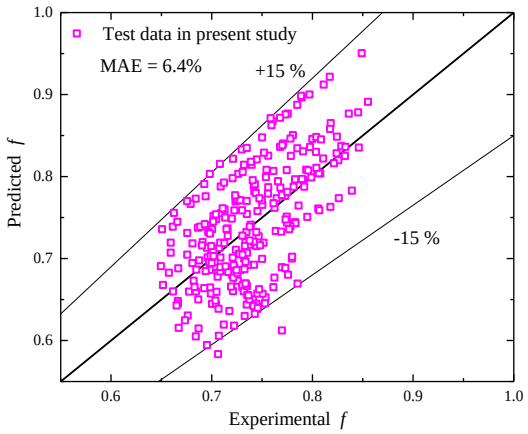

Figure 13 Comparison of proposed correlation (Eq. [31]) with present experimental data for Fanning friction factor

In order to evaluate the accuracy Eq. [23], similar experiments (using the same test rig) with high saturation temperatures using the working fluids R245fa and R1233zd were conducted. The working conditions are listed in Table 6. The predicted values of heat transfer coefficients and Fanning friction factors, which are calculated by two correlations derived in the present study, Eq. (23) and Eq. (31), respectively, are compared with experimental values obtained for the fluids R245fa and R1233zd in Figure 14. This comparison suggests that the correlations developed in the present study can predict with a good accuracy the experimental data obtained for R245fa and R1233zd as well.

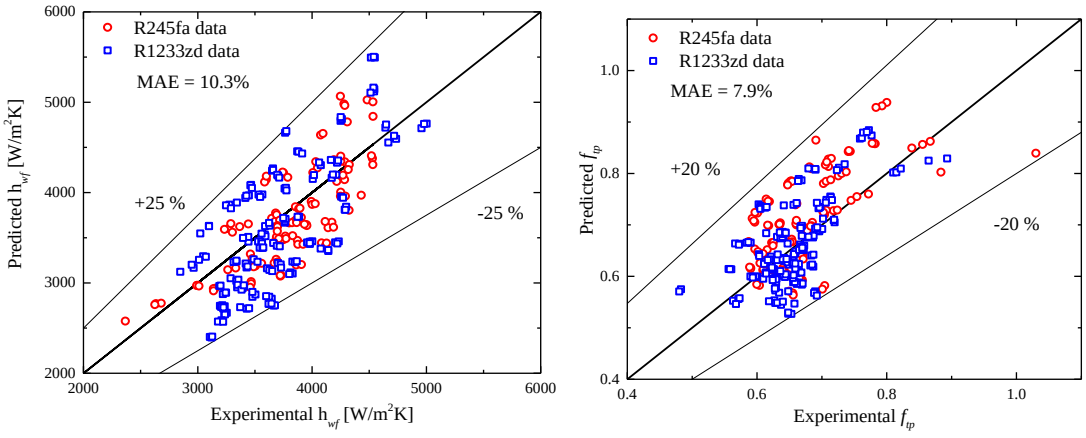

Figure 14 Comparison of experimental data of R245fa and R1233zd with predicted

values calculated using Eq. (23) and Eq. (31)

Table 6 Working conditions for R245fa and R1233zd

Working fluid	P_r	T_{sat} (°C)	G (kg/m^{3}s)	q (kW/m^2)	x_{in}	x_{out}
R245fa	0.34 - 0.65	100 - 130	56 – 103	10 - 37	0.03 - 0.61	0.51 - 1
R1233zd	0.29 - 0.54	100 - 130	60 – 103	9 - 38	0.05 - 0.42	0.44 - 1

Considering the experimental conditions and analysis outlined previously, the new heat transfer and pressure drop correlations are expected to apply for nucleate boiling dominant flow boiling in brazed PHEs in general. However, in order to draw more precise conclusions about the applicability of the new correlations, the correlations need to be thoroughly evaluated using numerous experimental data obtained for different working conditions and different PHE geometries.

5. Conclusions

An experimental investigation was conducted to study the flow boiling heat transfer and pressure drop performances of R134a, R1234yf and R1234ze at high saturation temperatures in a plate heat exchanger. The experimental data were tested with saturation temperatures of 60 °C, 70 °C and 80 °C (with corresponding reduced pressures of 0.35–0.74), mass fluxes of 86–137 kg/m^{2}s, heat fluxes of 9.8–36.8 kW/m^2 and outlet vapour qualities of 0.5–1. The key findings from the results are the following:

(1) Heat transfer coefficients are strongly dependent on the heat flux and saturation temperatures (reduced pressures). The experimental results suggest that the flow boiling in this study belongs to the nucleate boiling heat transfer

region and that the nucleate boiling is difficult to be suppressed at high saturation temperature.

(2) The frictional pressure drop increases with the increase of the mass flux and vapour quality and the decrease of saturation temperature.

(3) Seen from a thermal-hydraulic performance perspective, the results obtained in this paper indicate that R1234yf is a suitable replacement for R134a. This statement is attributed to the higher heat transfer coefficients and the lower frictional pressure drop of R1234yf compared with those of R134a.

(4) A new heat transfer correlation was developed based on the linear interpolation of the nucleate boiling [30] and saturated vapour heat transfer [36], and our results were predicted with a mean absolute error of 5.8 %.

(5) A new pressure drop correlation was developed based on a refitting of the Yan and Lin correlation [34], and our results were predicted with a mean absolute error of 6.4 % in terms of the two-phase Fanning friction factor.

Acknowledgement

The research leading to the research presented in this paper has received funding from the People Programme (Marie Curie Actions) of the European Union's Seventh Framework Programme (FP7/2007-2013) under the REA grant agreement n° 609405 (COFUNDPostdocDTU), and Innovationsfonden with the THERMCYC project (www.thermcyc.mek.dtu.dk, project ID: 1305-00036B). The financial support is gratefully acknowledged.

References

[1] J. Bao, L. Zhao, "A review of working fluid and expander selections for organic Rankine cycle," Renewable and Sustainable Energy Reviews, 24 (2013) 325-342.

[2] S. Quoilin, M. V. D. Broek, S. Declaye, P. Dewallef, V. Lemort, "Techno-economic survey of Organic Rankine Cycle (ORC) systems," Renewable and Sustainable Energy Reviews, 22 (2013) 168-186.

[3] R. L. Amalfi, F. Vakili-Farahani, J. R. Thome, "Flow boiling and frictional pressure gradients in plate heat exchangers. Part 1: Review and experimental database," International Journal of Refrigeration, 61 (2016) 166-184.

[4] Usman Muhammad, Muhammad Imran, Dong Hyun Lee, Byung Sik Park, "Design and experimental investigation of a 1 kW organic Rankine cycle system using R245fa as working fluid for low-grade waste heat recovery from steam," Energy Conversion and Management, 103 (2015) 1089-1100.

[5] Hyung-Chul Jung, Leighton Taylor, Susan Krumdieck, "An experimental and modelling study of a 1 kW organic Rankine cycle unit with mixture working fluid," Energy 81 (2015) 601-614.

[6] Yuping Wang, Xing Liu, Xiaoyi Ding, Yiwu Weng, "Experimental investigation on the performance of ORC power system using zeotropic mixture R601a/R600a," International Journal of Energy Research, 2016.

[7] Guoquan Qiu, Yingjuan Shao, Jinxing Li, Hao Liu, Saffa .B. Riffat, "Experimental investigation of a biomass-fired ORC-based micro-CHP for domestic applications," Fuel 96 (2012) 374–382.

[8] Y. Y. Hsieh, T. F. Lin, "Evaporation heat transfer and pressure drop of refrigerant

R-410A in a vertical plate heat exchanger," Journal of Heat Transfer, 125 (2003) 852-857.

[9] E. Djordjevic, S. Kabelac, "Flow boiling of R134a and ammonia in a plate heat exchanger," International Journal of Heat and Mass Transfer, 51 (2008) 6235-6242.

[10] F. Vakili-Farahani, R. L. Amalfi, J. R. Thome, "Two-phase flow and boiling of R245fa in a 1 mm pressing depth plate heat exchanger – Part II: flow boiling heat transfer," Interfacial Phenomena and Heat Transfer, 2 (2014) 343–361.

[11] M. S. Khan, T. S. Khan, Chyu, M. C., Ayub, Z. H., 2014, "Evaporation heat transfer and pressure drop of ammonia in a mixed configuration chevron plate heat exchanger," Int. J. Refrig., 41, pp. 92-102.

[12] V. Solotych, D. Lee, J. Kim, R. L. Amalfi, J. R. Thome, "Boiling heat transfer and two-phase pressure drops within compact plate heat exchangers: Experiments and flow visualizations," International Journal of Heat and Mass Transfer, 94 (2016) 239-254.

[13] J. Huang, T. J. Sheer, M. Bailey-McEwan, "Heat transfer and pressure drop in plate heat exchanger refrigerant evaporators," International Journal of Refrigeration, 35 (2012) 325-335.

[14] E. Lee, H. Kang, Y. Kim, "Flow boiling heat transfer and pressure drop of water in a plate heat exchanger with corrugated channels at low mass flux conditions," International Journal of Heat and Mass Transfer, 77 (2014) 37-45.

[15] D. Han, K. Lee, Y. Kim, "Experiments on the characteristics of evaporation of R410A in brazed plate heat exchangers with different geometric configurations,"

Applied Thermal Engineering, 23 (2003) 1209-1225.

[16] G.A. Longo, "Hydrocarbon Refrigerant Vapourization Inside a Brazed Plate Heat Exchanger," Journal of Heat Transfer, 134 (2012) 101801.

[17] W. Liu, D. Meinel, C. Wieland, H. Spliethoff, "Investigation of hydrofluoroolefins as potential working fluids in organic Rankine cycle for geothermal power generation," Energy, 67 (2014) 106-116.3

[18] J. S. Brown, "HFOs New, Low Global Warming Potential Refrigerants," Ashrae Journal, 51 (2009) 22-29.

[19] G. A. Longo, C. Zilio, "Condensation of the low GWP refrigerant HFC1234yf inside a brazed plate heat exchanger," International Journal of Refrigeration, 26 (2013) 612-621.

[20] H. Martin, "A theoretical approach to predict the performance of chevron-type plate heat exchangers," Chemical Engineering and Processing 35 (1996) 301-310.

[21] R.K. Shah, "Assessment of modified Wilson plot techniques for obtaining heat exchanger design data," Proceedings of the Ninth International Heat Transfer Conference, Jerusalem, Israel, 5 (1990) 51-56.

[22] VDI Heat Atlas, Second Edition, Springer, 2010.

[23] B. Thonon, R. Vidil, C. Marvillet, "Recent research and developments in plate heat exchangers," Journal of Enhanced Heat Transfer, 2 (1995) 149-155.

[24] J. R. Thome, "Encyclopedia of Two-Phase Heat Transfer and Flow I Fundamentals and Methods", World Scientific Publishing Co Pte Ltd, 2015.

[25] J. G. Collier, J. R. Thome, "Convective Boiling and Condensation", third Edition,

Oxford University Press, 1994.

[26] D. S. Jung, M. Mclinden, R. Radermachert, D. Didion, "Horizontal flow boiling heat transfer experiments with a mixture of R22/R114," International Journal of Heat and Mass Transfer, 32 (1989) 131-145.

[27] H. Ross, R. Radermacher, M. Marzo, D. Didion, "Horizontal flow boiling of pure and mixed refrigerants," International Journal of Heat and Mass Transfer, 30 (1987) 979-992.

[28] C. S. Brooks, N. Silin, T. Hibiki, M. Ishii, "Experimental investigation of wall nucleation characteristics in flow boiling," Journal of Heat Transfer, 137 (2015) 051501.

[29] R. L. Amalfi, F. Vakili-Farahani, J. R. Thome, "Flow boiling and frictional pressure gradients in plate heat exchangers. Part 2: Comparison of literature methods to database and new prediction methods," International Journal of Refrigeration, 61 (2016) 185-203.

[30] M. G. Cooper, "Flow boiling-the 'apparently nucleate' regime," International Journal of Heat and Mass Transfer, 32 (1989) 459-464.

[31] V. D. Donowski, S. G. Kandlikar, "Correlating evaporation heat transfer coefficient of refrigerant R-134a in a plate heat exchanger," Engineering Foundation Conference on Pool and Flow Boiling, Alaska, Paper 154, 2000.

[32] J. H. Park, Y. S. Kim, "Evaporation heat transfer and pressure drop characteristics of R134a in the oblong shell and plate heat exchanger," KSME International Journal, 18 (2004) 2284-2293.

[33] Hsieh, Y. Y., Lin, T. F., 2002, "Saturated flow boiling heat transfer and pressure

drop of refrigerant R410A in a vertical plate heat exchanger," International Journal of Heat and Mass Transfer, 45 (2002) 1033-1044.

[34] Yan, Y.Y., and Lin, T.F., 1999, "Evaporation Heat Transfer and Pressure Drop of Refrigerant R-134a in a Plate Heat Exchanger," Journal of Heat Transfer, 121 (1999) 118-127.

[35] Incropera, F. P., and DeWitt, D. P., Introduction to Heat Transfer, John Wiley & Sons, New York, 1996.

[36] Mori, H., Yoshida, S., Ohishi, K., Kokimoto, Y., "Dryout quality and post dryout heat transfer coefficient in horizontal evaporator tubes," in: Proc of 3rd European Thermal Sciences Conference, 839–844, 2000.